Asian Journal of Chemistry; Vol. 38, No. 6 (2026), 1439-1446
ASIAN JOURNAL OF CHEMISTRY
https://doi.org/10.14233/ajchem.2026.35380

Evaluation of Millet Extract as Green Inhibitor for AA6063 Corrosion in 1 M KCl: From Electrochemical Studies to Optimisation

OJO S.I. FAYOMI[1,2], ONYEKA G. OGBUOZOBE[1,*] and HO SOON MIN[3]

[1]Department of Mechanical Engineering, Bells University of Technology, P.M.B. 1015, Ota, Ogun State, Nigeria
[2]Department of Mechanical Engineering Science, University of Johannesburg, Auckland Park, Kingsway Campus, P.O. Box 534, Johannesburg, South Africa
[3]Faculty of Health and Life Sciences, INTI International University, Putra Nilai, 71800, Negeri Sembilan, Malaysia

*Corresponding author: E-mail: godsononyeka507@gmail.com

Received: 2 December 2025 *Accepted*: 17 April 2026 *Published online*: 31 May 2026 AJC-22370

This study presents a comprehensive evaluation of millet extract as a green corrosion inhibitor for the protection of AA6063 in a 1 M KCl solution medium. The research integrates multiple electrochemical techniques, including open circuit potential (OCP) measurements and linear sweep voltammetry (LSV), alongside detailed adsorption studies. These are further complemented by the application of response surface methodology (RSM) to enhance and optimize the inhibitor's performance. A central composite design (CCD) was strategically employed to systematically vary key experimental parameters, specifically, the concentration of millet extract and the operating solution temperature. The electrochemical investigations provided deeper insights into the underlying inhibition mechanism, while the RSM framework enabled the identification of optimal operating conditions for corrosion control. The resulting second-order polynomial model was rigorously validated through analysis of variance (ANOVA), which confirmed the statistical significance and strong influence of both concentration and temperature on the corrosion rate. The optimal conditions were determined at a concentration of 0.284 g and a temperature of 33.56 ºC, resulting in a low corrosion rate of 0.332 mm yr^{-1}. This study concludes that millet extract is an effective and environmentally friendly corrosion inhibitor, offering a viable, sustainable alternative to conventional chemical inhibitors in corrosion prevention strategies.

Keywords: Aluminium alloy, Corrosion, Inhibition, Millet extract, Optimisation, Industrial growth.

INTRODUCTION

AA6063 is an aluminium alloy that has gained widespread industrial use due to its excellent extrudability, moderate strength, good weldability and resistance to various types of corrosion [1]. The alloy finds numerous applications including furniture, doors, architectural extrusions, pipes, window frames, road transport, rail transport, truck and trailer floors as well as hospital and medical equipment [2]. Aluminium is favoured in the industry for power transmission and metallurgy applications due to its high electrical conductivity, good working and forming properties, lightness, ease of recycling, low density, ductility and high mechanical strength [3]. Despite these favourable properties, AA6063 suffers from corrosion in acidic environments that hampers industrial growth [4,5]. When AA6063 is exposed to acidic solutions, the corrosion mechanism involves the destruction of the naturally formed protective oxide layer on the aluminium surface [6]. Plant extracts have thus emerged as effective green corrosion inhibitors for AA6063 in acidic environments, offering a non-toxic and cost-effective alternative to traditional inhibitors [7].

Recent advances in nanomaterials have also demonstrated that metal oxide nanoparticles possess significant potential for environmental and technological applications [8]. Arecanut seed extracts have shown significant inhibition properties for aluminium in 0.5 M HCl. Both ethyl acetate extract from mature arecanut seed (EEMAS) and water extract from mature arecanut seed (WEMAS) were reported to effectively hinder both anodic and cathodic reactions at active metal surface sites. The maximum shifts in corrosion potential were 22 mV for EEMAS and 78 mV for WEMAS, indicating that these inhibitors work through a mixed mode of inhibition by retarding both anodic dissolution and cathodic evolution reactions [9]. In chloride environments, *Prunus domestica* extract demonstrated exceptional performance for AA6063-T5 aluminium alloy in 3.5 wt.% NaCl solution, achieving 99.01% inhibition

TABLE-1
ELEMENTAL COMPOSITION OF AA6063 ALUMINIUM ALLOY SPECIMEN (% BY WEIGHT)

Elements	Zn	Fe	Si	Mg	Ti	Cu	Mn	Al
Weight %	< 0.05	0.23	0.39	0.69	0.03	0.028	0.087	Bal.

efficiency [10]. While extensive research has been conducted on various plant extracts as corrosion inhibitors for AA6063, specific studies on millet extract for this particular aluminium alloy in KCl are limited. Thus, the study seeks to investigate the inhibition capacity of millet extract for AA6063 in 1 M KCl.

EXPERIMENTAL

AA6063 samples preparation: The research made use of AA6063 from a supplier in Ota, Ogun State, Nigeria. The elemental composition is detailed in Table-1. Samples (20 mm × 20 mm × 3 mm), were cut from the stock with a hacksaw. They were ground from P60 to P320, then polished with P600 to P2000 to achieve a mirror finish. The polishing protocol was standardised and repeated for all samples to ensure consistent surface finish and reproducibility across experiments. The coupons were cleaned in distilled water, degreased with acetone and dried before use.

Preparation of millet extract inhibitor: Pearl millet (*Pennisetum glaucum*) grains were first cleaned to remove dirt and foreign materials, then air-dried at ambient temperature for 48 h. The dried grains were ground into a fine powder using a laboratory blender. About 100 g of powdered millet was soaked in 500 mL of ethanol–water mixture (70:30 v/v) and allowed to macerate for 72 h at room temperature with intermittent stirring to enhance the extraction of active phytochemicals such as flavonoids, phenolics and alkaloids. After maceration, the solution was filtered through Whatman No. 1 filter paper to remove solid residues. The filtrate was concentrated using a rotary evaporator at 50 ºC to remove the solvent, yielding a viscous brown extract, which was preserved in an airtight container and refrigerated until required for corrosion inhibition studies in 1 M KCl medium. The phytochemical composition of the extract is shown in Table-2.

TABLE-2
LIST OF PHYTOCHEMICALS PRESENT IN MILLET EXTRACT

Phytochemical compound	Confirmation
Phenol	Absent
Terpenoids	Absent
Protein	Absent
Coumarins	Abundance
Saponins	Abundance
Tannins	Absent
Steroids	Absent
Alkaloids	Absent
Flavonoids	Absent
Reducing sugar	Present

Electrochemical set-up: For the assessment of the corrosion inhibition efficacy of Millet extract on AA6063 in 1 M KCl solution, a systematic experimental protocol was implemented. The study encompassed the immersion of AA6063 coupons in 50 mL of electrolyte under both uninhibited and inhibited conditions, with inhibitor volumes varying from 0.0 mL to 0.3 mL. The temperature was precisely regulated at 30, 40 and 50 ºC to scrutinize its influence on corrosion dynamics. Electrochemical characterisation was performed utilizing a CS100 Potentiostat with a standard three-electrode system comprising an AA6063 working electrode (1 cm^2), a saturated Ag/AgCl reference electrode and a graphite auxiliary electrode. All electrochemical measurements were performed in triplicate to ensure repeatability and average values are reported. Potentiodynamic polarisation curves were recorded spanning -1.5 V to +1.5 V *versus* SCE at a scanning rate of 0.01 V s^{-1}. The scan rate of 0.01 V s^{-1} was selected to minimize ohmic drop and ensure quasi-steady-state conditions, as recommended in standard corrosion testing protocols. IR compensation was performed using the built-in positive feedback function of the potentiostat to minimise the effect of solution resistance during electrochemical measurements. Homogeneity of the inhibitor-laden electrolyte was ensured by magnetic stirring prior to electrochemical measurements. Sample preparation involved mechanical abrasion with 1200-grit emery paper, followed by ultrasonic cleaning in deionised water to eliminate surface impurities. Following preparation, coupons were allowed to equilibrate in the electrolyte for 120 sec to attain a steady-state open circuit potential (OCP) before any electrochemical measurement. Post-preparation, coupons were soaked in the electrolyte for 120 sec to attain a steady-state open circuit potential. Tafel analysis was pivotal in scrutinyzing the electrochemical corrosion properties of the examined material. This method enabled the precise determination of critical parameters including the corrosion potential (E_{corr}), which signifies the corrosion driving force and the corrosion current density (j_{corr}) which is indicative of the corrosion rate. The surface coverage, a metric for the extent of the surface shielded by the inhibitor, was also quantified. The inhibition efficiency (IE%) was ascertained utilizing eqns. 1 and 2, providing a quantitative measure of the inhibitor's effectiveness. Furthermore, the three major adsorption isotherm models, namely Langmuir, Freundlich and Temkin were applied to the experimental data to ascertain the most suitable model for characterizing the inhibitor's adsorption onto the material surface. Lastly, the topographical examination of the corrosion inhibited AA6063 samples was performed using metallurgical microscopy.

$$\text{Surface coverage } (\theta) = \frac{J^{o}_{corr} - J_{corr}}{J^{o}_{corr}} \quad (1)$$

$$\text{IE } (\%) = \frac{J^{o}_{corr} - J_{corr}}{J^{o}_{corr}} \times 100 \quad (2)$$

RESULTS AND DISCUSSION

Response of test AA6063 samples to corrosion inhibition: The time-dependent OCP plots at 30 ºC, 40 ºC and 50 ºC (Figs. 1a, 2a and 3a) provide initial insights into the thermo-

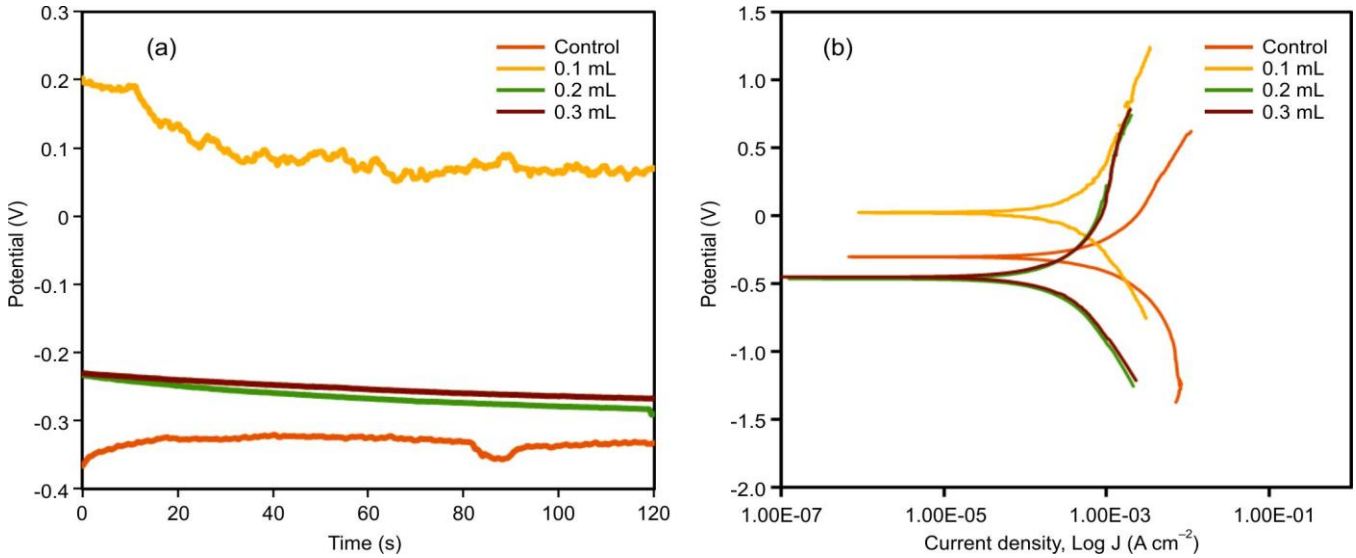

Fig. 1. OCP and LSV plots of millet extract inhibited samples at 30 ºC

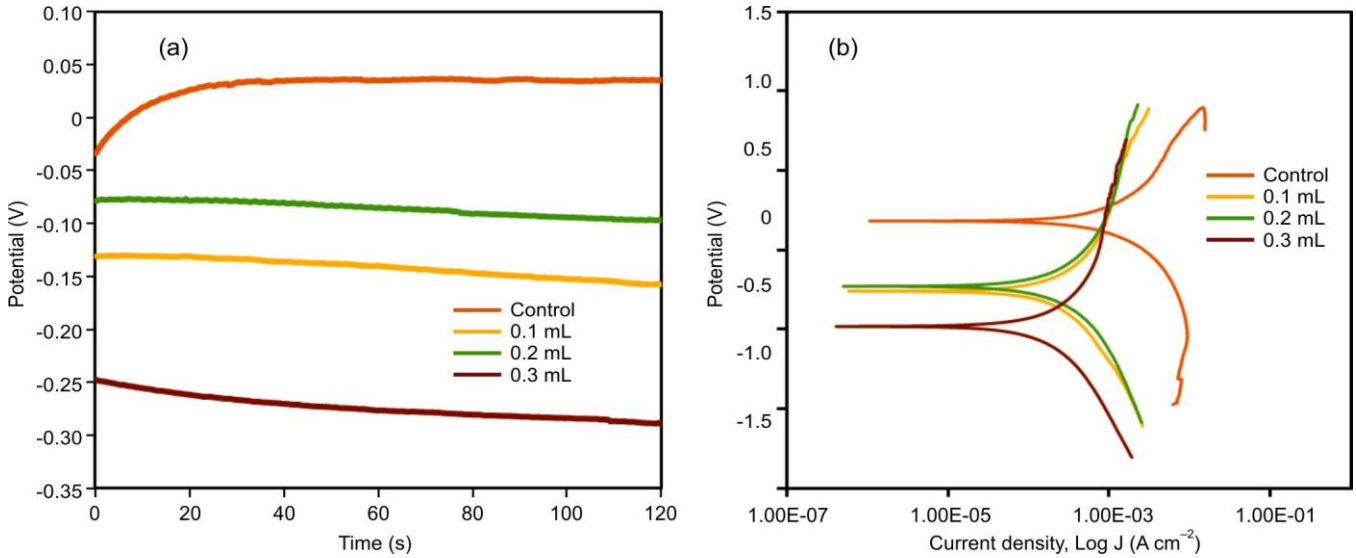

Fig. 2. OCP and LSV plots of millet extract inhibited samples at 40 ºC

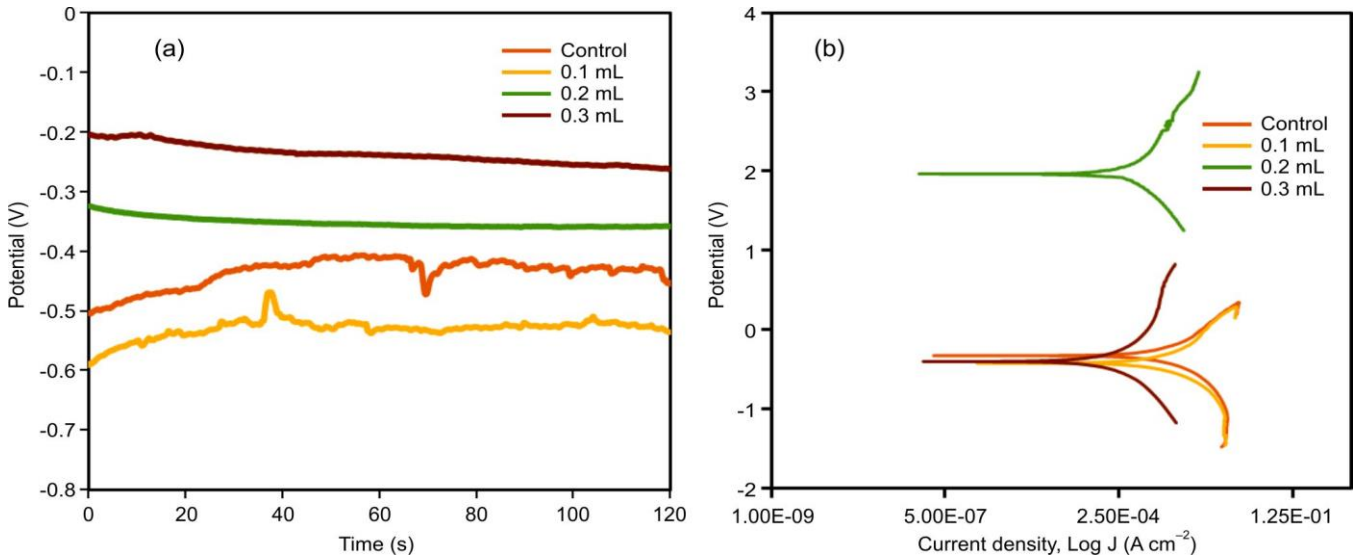

Fig. 3. OCP and LSV plots of millet extract inhibited samples at 50 ºC

dynamic tendencies of the AA6063 surface in the presence and absence of Millet extract. At 30 ºC (Fig. 1a), the control sample exhibited the most negative and unstable potential. At 40 ºC (Fig. 2a), the OCP trends reversed slightly. The control now exhibited a relatively positive potential (~+0.05 V), while the inhibited systems shifted cathodically, especially at 0.3 mL, which dropped to approximately -0.32 V. This behaviour points to enhanced cathodic inhibition at elevated temperatures, likely due to the stronger adsorption of phytochemicals onto the metal surface, forming a more protective barrier as temperature increases [11]. The 0.1 mL and 0.2 mL samples exhibited intermediate OCP values confirming concentration-dependent inhibitor interaction [12].

At 50 ºC (Fig. 3a), the inhibited samples exhibited corrosion potentials within the expected electrochemical range for AA6063 in 1 M KCl, with the 0.2 mL inhibitor concentration showing an OCP of –0.23 V. The control, 0.1 mL and 0.3 mL samples clustered around ~–0.4 V, indicating consistent corrosion activity. The sharp contrast between the 0.2 mL sample and the rest suggests non-linear adsorption dynamics or temperature-activated synergistic effects within the extract components at this specific concentration.

The polarisation curves (Figs. 1b, 2b and 3b) provide kinetic insights into corrosion behaviour. At 30 ºC (Fig. 1b), the control exhibited a relatively high corrosion current density (J_{corr} = 1.90×10^{-4} A cm^{-2}) with a corrosion potential (E_{corr}) of –0.302 V. The addition of 0.1 mL of Millet extract caused a notable anodic shift to +0.024 V and a reduction in J_{corr} to 8.56×10^{-5} A cm^{-2}, suggesting mixed-type inhibition with a stronger anodic component [13]. For 0.2 mL and 0.3 mL, more negative E_{corr} values (–0.464 V and –0.451 V) were recorded with even lower J_{corr} values (5.25×10^{-5} and 4.98×10^{-5} A cm^{-2} respectively), implying cathodic dominance and improved barrier formation with increasing concentration [14]. The polarisation resistance (PR) also increased with concentration, reaching a maximum of 522 Ω at 0.3 mL, reinforcing the effectiveness of the extract at this dose. At 40 ºC (Fig. 2b), the control's J_{corr} further increased to 2.89×10^{-4} A cm^{-2} with a relatively positive E_{corr} of +0.181 V, suggesting temperature-enhanced corrosion kinetics. However, all inhibited systems showed improved performance, with the 0.3 mL sample showing the lowest J_{corr} (4.51×10^{-5} A cm^{-2}) and highest PR (577 Ω). The E_{corr} values of the inhibitors shifted negatively, particularly at 0.3 mL (–0.482 V), confirming the cathodic nature of inhibition at the elevated temperatures [15]. This cathodic suppression limits hydrogen evolution and electron transfer, thereby reducing corrosion rates even at elevated kinetic energy states. At 50 ºC (Fig. 3b), corrosion activity escalated for the control and 0.1 mL concentrations, with J_{corr} of 3.52×10^{-4} and 3.46×10^{-4} A cm^{-2} respectively and minimal resistance values (~74-75 Ω), indicating ineffective inhibition. However, 0.2 mL sample exhibited a corrosion potential of –0.230 V and a reduced corrosion current density of 1.27×10^{-4} A cm^{-2}, indicating improved inhibition compared with the uninhibited system [16]. The 0.3 mL sample, with an E_{corr} of –0.400 V and J_{corr} of 4.70×10^{-5} A/cm^2, restored stability and yielded a high polarization resistance of 553 Ω, confirming that the inhibition efficiency peaks at this concentration regardless of elevated temperature [17].

The Tafel data (Table-3) confirms and complements both the OCP and LSV interpretations. At 30 ºC, corrosion rate (CR) decreased from 2.23 mm yr^{-1} in the control to 0.58 mm yr^{-1} at 0.3 mL, marking a ~74% reduction. The polarization resistance trend increased with concentration, with values of 137 Ω (control) rising to 522 Ω at 0.3 mL, signifying more resistive and less conductive surface interfaces. E_{corr} values suggest a dual mechanism while 0.1 mL produced an anodic shift, higher concentrations induced cathodic shifts, aligning with mixed-type inhibition that leans cathodic at higher dosages. At 40 ºC, the same inhibition trend persisted, with CR reducing from 3.39 mm yr^{-1} (control) to 0.53 mm yr^{-1} at 0.3 mL. The sharp decline in J_{corr} across all inhibitor doses reflects strong inhibitory film stability at this temperature [18], with enhanced resistance values (>570 Ω) suggesting persistent surface protection. The E_{corr} shifts were predominantly cathodic, further substantiating cathodic suppression as the main mechanism at elevated temperatures. At 50 ºC, the control and 0.1 mL cases showed poor performance (CR ~4.1 mm yr^{-1}), while the 0.3 mL treatment again demonstrated the best inhibition, lowering the CR to 0.55 mm yr^{-1}. The 0.2 mL sample displayed a high E_{corr} (1.964 V), but a low J_{corr} (1.27×10^{-4} A cm^{-2}) and a high polarization resistance of 205 Ω, implying the formation of a highly stable passive layer [19]. The corrosion potentials (E_{corr}) of AA6063 in the presence of millet extract exhibit both anodic and cathodic shifts depending on inhibitor concentration. At 30 ºC, addition of 0.1 mL extract shifted E_{corr} anodically to +0.024 V, while higher concentrations (0.2 mL and 0.3 mL) shifted E_{corr} cathodically to –0.464 V and –0.451 V, respectively. Concurrently, corrosion current density (J_{corr}) decreased from 1.90×10^{-4} A cm^{-2} for control to 8.56×10^{-5} A cm^{-2} at 0.1 mL and further to 5.25×10^{-5} and 4.98×10^{-5} A cm^{-2} at 0.2 mL and 0.3 mL, respectively. Polarisation resistance increased from 137 Ω (control) to 304 Ω at 0.1 mL and reached 522 Ω at 0.3 mL. Similar trends were observed at 40 ºC, with E_{corr} values shifting from –0.260 V to –0.482 V and J_{corr} decreasing from 6.71×10^{-5} A cm^{-2} to 4.51×10^{-5} A cm^{-2} as inhibitor concentration increased, while polarization resistance increased from 387 Ω to 577 Ω. These results indicate mixed type inhibition across the temperature range, with higher inhibitor doses producing a stronger cathodic effect,

TABLE-3
RESULTS OF TAFEL POLARIZATION STUDIES OF AA6063 ALUMINIUM ALLOY IN MILLET EXTRACT

Samples	E_{corr} (V)			J_{corr} (A/Cm^2)			CR (mm/yr)			PR (Ω)		
	30 ºC	40 ºC	50 ºC	30 ºC	40 ºC	50 ºC	30 ºC	40 ºC	50 ºC	30 ºC	40 ºC	50 ºC
Control	-0.302	0.181	-0.326	1.90E-04	2.89E-04	3.52E-04	2.23	3.39	4.12	1.37E+02	8.99E+01	7.40E+01
0.1 mL	0.024	-0.260	-0.419	8.56E-05	6.71E-05	3.46E-04	1.00	0.79	4.06	3.04E+02	3.87E+02	7.51E+01
0.2 mL	-0.464	-0.230	-0.230	5.25E-05	6.16E-05	1.27E-04	0.62	0.72	1.49	4.95E+02	4.22E+02	2.05E+02
0.3 mL	-0.451	-0.482	-0.400	4.98E-05	4.51E-05	4.70E-05	0.58	0.53	0.55	5.22E+02	5.77E+02	5.53E+02

as evidenced by the more negative E_{corr} values and increased polarization resistance. At 50 ºC, the 0.2 mL and 0.3 mL samples maintained low J_{corr} values (1.27×10^{-4} A cm^{-2} and 4.70×10^{-5} A cm^{-2}) and elevated polarization resistance (205 Ω and 553 Ω), confirming effective inhibition and predominance of cathodic suppression at higher concentrations. These findings underscore a thermally activated, concentration specific adsorption behaviour of millet extract constituents, possibly due to synergistic interactions between flavonoids, phenolics or other active compounds.

Millet extract inhibitory efficiency: The inhibition efficiency plot (Fig. 4) offers a direct reflection of the protective performance of millet extract at varying concentrations and temperatures. At 30 ºC, the efficiency increased with concentration, rising from 55.16% at 0.1 mL to 73.99% at 0.3 mL. This suggests increasing surface coverage and barrier formation on AA6063 as the phytochemical content in the solution increases. At 40 ºC, the trend was similar but slightly enhanced: 76.7%, 78.76% and 84.37% were recorded for 0.1, 0.2 and 0.3 mL respectively. While the efficiency plateaued beyond 0.1 mL, the values still indicate sustained inhibitor performance despite the elevated temperature. However, at 50 ºC, the inhibition behaviour becomes more concentration-sensitive. A sharp decline was observed at 0.1 mL (1.46%), possibly due to thermal desorption or breakdown of inhibitor components. At 0.2 mL, the inhibition efficiency recovered to 63.83% and reached 86.65% at 0.3 mL, the highest across all conditions. This nonlinear behaviour reinforces the need for sufficient dosage to overcome thermally driven desorption or competitive adsorption by aggressive ions (*e.g.* Cl^-). The data strongly correlate with the electrochemical findings, where 0.3 mL consistently yielded the highest polarisation resistance (PR), lowest corrosion rate (CR) and most stable OCP behaviour.

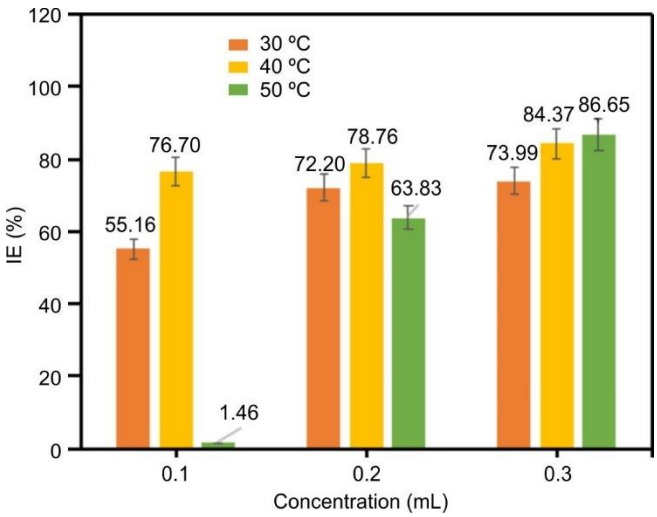

Fig. 4. Inhibitor efficiency plot of millet extract on AA06063

Adsorption response of inhibited AA6063 samples: The Langmuir model assumes monolayer adsorption on a homogenous surface without interactions between adsorbed species [20]. It provided excellent correlation at 30 ºC (R^2 = 0.9929) and 40 ºC (R^2 = 0.9969) in Table-4, suggesting that under these conditions, the inhibition process follows ideal monolayer

TABLE-4
LANGMUIR AND FREUNDLICH ADSORPTION ISOTHERMs PARAMETERS FOR MILLET EXTRACT ADSORPTION ON AA6063

Temp. (ºC)	Langmuir adsorption isotherm		Freundlich adsorption isotherm	
	K_{ads} (mol^{-1})	R^2	K_{ads} (mol^{-1})	R^2
30	15.6811	0.9929	1.0735	0.9137
40	46.6692	0.9969	0.9179	0.8482
50	0.1108	0.7462	156.6344	0.9090

adsorption. The corresponding K_{ads} values; 15.6811 mol^{-1} (30 ºC) and 46.6692 mol^{-1} (40 ºC) indicate moderate to strong binding, implying chemisorption tendencies. However, at 50 ºC, the fit to the Langmuir model deteriorated sharply (R^2 = 0.7462, K_{ads} = 0.1108 mol^{-1}), suggesting deviation from monolayer behaviour due to temperature-induced desorption, multilayer adsorption or surface heterogeneity. The Freundlich isotherm, applicable to heterogeneous surfaces and multilayer adsorption [21], showed weaker correlation in Table-4, especially at 40 ºC (R^2 = 0.8482) compared to 30 ºC (R^2 = 0.9137). Notably, the K_{ads} at 50 ºC increase sharply to 156.63, which seems counterintuitive but aligns with the θ *vs.* ln C plot (Fig. 5), where surface coverage increased non-linearly with concentration. This supports the idea that at higher temperatures, adsorption may involve complex mechanisms beyond single-layer binding, such as interfacial layering or dynamic equilibrium between adsorbed and desorbed species.

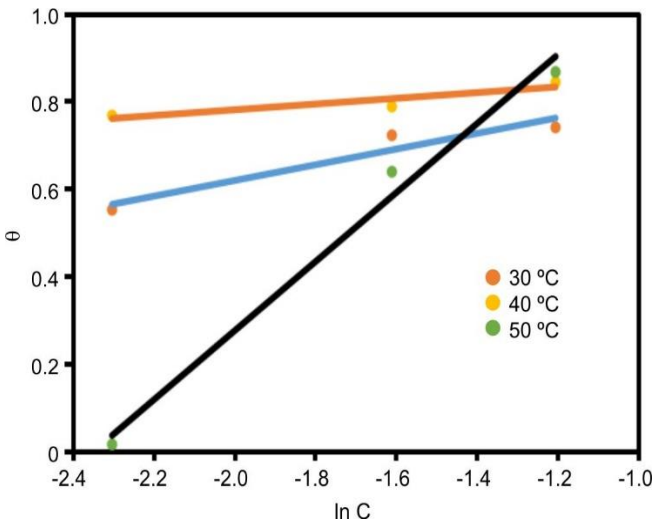

Fig. 5. Variation of surface coverage (θ) with concentration (ln C)

The Temkin isotherm incorporates adsorbate–adsorbate interactions and changes in adsorption energy [22]. Here, the adsorption data best fit this model at 50 ºC (R^2 = 0.9875) as shown in Table-5, despite its poor Langmuir fit, highlighting that at higher temperatures, surface interactions become more significant. The calculated ΔG_{ads} values for all temperatures were negative, confirming the spontaneity of adsorption.

According to standard interpretation, the values more negative than -20 kJ/mol typically suggest chemisorption, while those less negative imply physisorption. Thus, at 30 and 40 ºC, the adsorption mechanism is likely chemisorptive, involving charge transfer or chemical bonding of active cons-

TABLE-5
TEMKIN ISOTHERM ADSORPTION PARAMETERS FOR THE
INTERACTION BETWEEN MILLET EXTRACT AND AA6063 SURFACE

Temp. (ºC)	K_{ads} (mol^{-1})	ΔG_{ads} (KJ mol^{-1})	R^2	ln (K_{ads})	1/T	ΔG_{ads}/T	Slope (B)
30	231.6975	-23.8400	0.9198	5.4454	0.0033	-0.0787	0.1794
40	1098710.4722	-46.6570	0.8408	13.9096	0.0032	-0.1491	0.0655
50	10.4578	-17.0924	0.9875	2.3474	0.0031	-0.0529	0.7889

tituents to the metal surface. At 50 ºC, the lower ΔG_{ads} may indicate a partial transition toward physisorption, possibly due to thermal agitation disrupting chemisorptive interactions. The θ *vs.* ln C plot (Fig. 5) further clarifies the adsorption behaviour. At 30 ºC and 40 ºC, the near-linear increase in θ with ln C supports Langmuir-type behaviour consistent with their high R^2 values. However, the curve obtained at 50 ºC appears more scattered and less steep, indicating reduced adsorption stability and deviation from ideal adsorption behaviour. The black line (presumably theoretical Langmuir fit) highlights that only the lower temperature data align closely, while the 50 ºC data deviate significantly. This plot visually confirms that adsorption efficiency improves with concentration, but the mechanism becomes temperature-dependent, transitioning from monolayer chemisorption to potentially multilayer or competitive adsorption at higher temperatures.

Optical micrograph of corroded samples: Fig. 6a-d presents optical micrographs (magnified at 40×) illustrating the surface morphology of AA6063 specimens subjected to corrosive conditions, both without and with varying concentrations of millet extract as a corrosion inhibitor. In the uninhibited sample (Fig. 6a), the surface appears severely degraded, with pronounced corrosion damage and accumulation of corrosion products, highlighting the aggressive nature of 1 M KCl medium in the absence of protective agents. In contrast, Fig. 6b-c, corresponding to samples treated with increasing concentrations of millet extract, display relatively smoother surfaces with fewer corrosion-induced defects, indicating a noticeable reduction in surface deterioration. This visual improvement affirms the extract's corrosion mitigation potential through adsorption and film formation on the metal surface. Fig. 6d reveals that the specimen exposed to the highest inhibitor concentration maintains a comparatively smooth and intact morphology, supporting the electrochemical observations. Thus, the progressive improvement in surface integrity across the images supports the extract's efficacy in reducing corrosion attack on the AA6063.

Empirical optimisation: To investigate the combined effects of inhibitor concentration and temperature on corrosion rate, a response surface methodology (RSM) approach

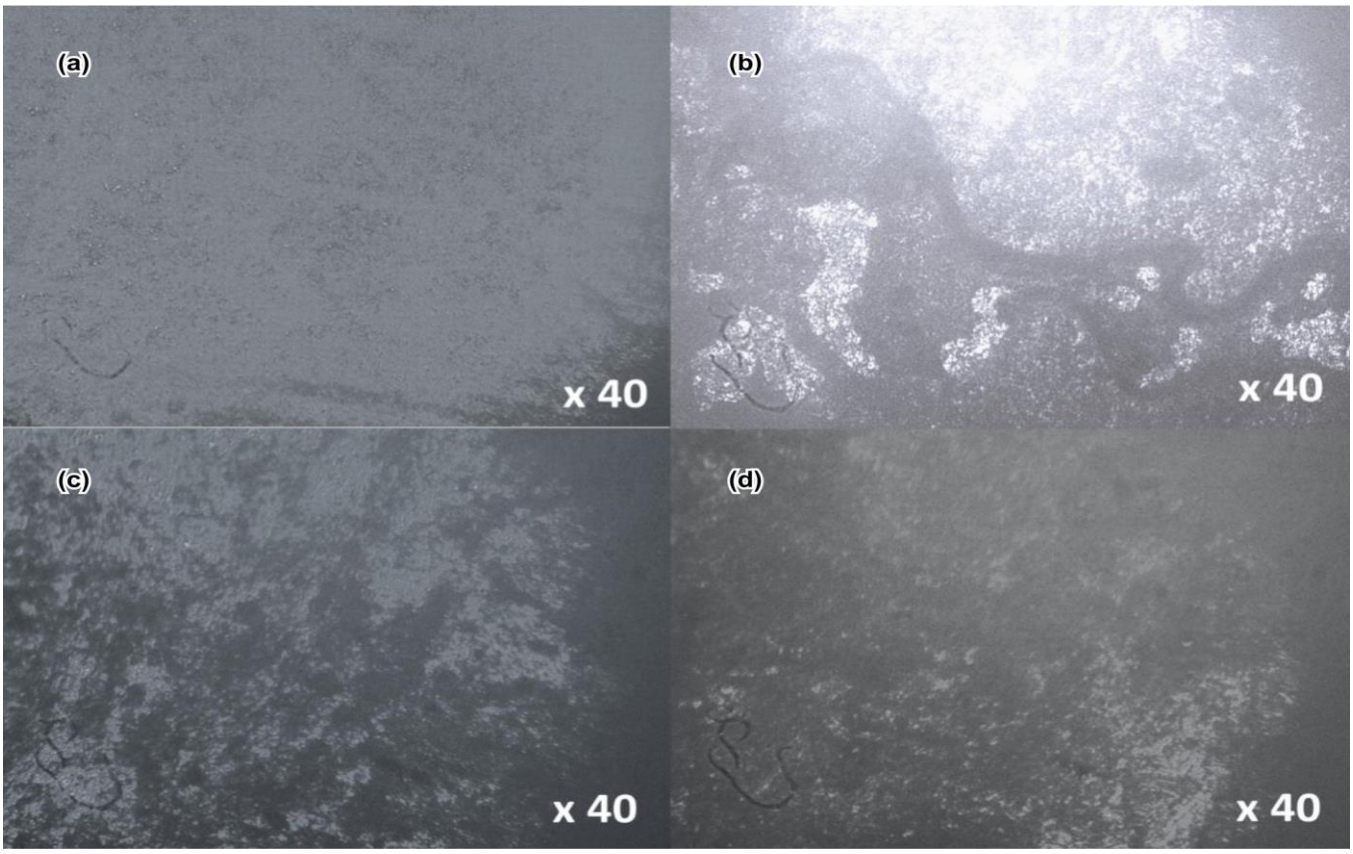

Fig. 6. Optical micrographs (40×) showing surface morphology of AA6063 at 50 ºC with and without millet extract (control, 0.1 mL, 0.2 mL, 0.3 mL)

TABLE-6
OPTIMISED CORROSION RESPONSE OF AA6063 TO MILLET
EXTRACT INHIBITION BASED ON ANOVA STATISTICAL ANALYSIS

Source	SS	DF	MS	F-value	*p*-value	Remark
Model	18.16	3	6.05	12.63	0.0021	Sig.
A-Conc.	12.39	1	12.39	25.85	0.0009	
B-Temp.	4.19	1	4.19	8.74	0.0182	
AB	1.58	1	1.58	3.3	0.1069	
Residual	3.83	8	0.4792			
Cor Total	21.99	11				

R^2 = 82.57%; Adjusted R^2 = 76.03%; predicted R^2 = 65.23%; CV%= 41.37: Std. Dev. 0.692; ** SS - sum of square; DF - degree of freedom; MS - mean square; Sig. - significant**

based on a central composite design (CCD) was employed. The CCD consisted of factorial points, axial points and centre point replicates, allowing estimation of linear, interaction and curvature effects while also providing an estimate of experimental error. The ANOVA response table (Table-6) obtained from the DOE Table presented in Table-7 indicates that the model is statistically significant, with a *p*-value of 0.0021. This suggests that the model explains a significant portion of the variability in the corrosion rate (CR). The R^2 value of 82.57% indicates that approximately 82.57% of the variability in the response can be explained by the model, which is a strong indication of the model's predictive power. The central composite design (CCD) employed included concentration (Factor A) and temperature (Factor B) as independent variables, with factorial points, axial points and replicates at the center point to ensure model robustness and allow estimation of experimental error. The individual factors, concentration (A) and temperature (B), both show significant effects on the corrosion rate, with *p*-values of 0.0009 and 0.0182, respectively. This means that changes in concentration and temperature significantly affect the corrosion rate of the material. The concentration factor has a higher F-value (25.85) compared to the temperature factor (8.74), suggesting that concentration has a stronger influence on the corrosion rate than temperature. The interaction term AB (concentration and temperature) has a *p*-value of 0.1069, which is greater than the commonly used significance level of 0.05. This indicates that the interaction between concentration and temperature is not statistically significant. Therefore, the effect of concentration on the corrosion rate does not depend on the temperature and *vice-versa*.

TABLE-7
DESIGN MATRIX OF PROCESS PARAMETERS
AND CORRESPONDING CORROSION RESPONSE

Factor A: Concentration (mL)	Factor B: Temperature (ºC)	Response: CR (mm/yr)
0	30	2.23
0.1	30	1.00
0.2	30	0.62
0.3	30	0.58
0	40	3.39
0.1	40	0.79
0.2	40	0.72
0.3	40	0.53
0	50	4.12
0.1	50	4.06
0.2	50	1.49
0.3	50	0.55

The predicted R^2 value of 65.23% is slightly lower than the adjusted R^2 value of 76.03%, indicating that the model fits the data well but may not predict new data as accurately as it explains the existing data. The coefficient of variation (CV%) of 41.37% reflects moderate variability primarily at extreme conditions (*e.g.* high temperature and low inhibitor concentrations) but does not compromise the reliability of model across the majority of the experimental domain.

The 3D plot (Fig. 7) of the response surface provided shows the response surface for the corrosion rate as a function of concentration and temperature. The surface plot illustrates the influence of both variables on the corrosion rate. A clear decrease in corrosion rate is observed with increasing concentration, consistent with the trend identified in the ANOVA results. From the optimisation ramp plot (Fig. 8), the optimal conditions for minimizing the corrosion rate appear to be at higher concentrations and moderate temperatures. The lowest point on the surface, which represents the minimum corrosion rate, occurs at a concentration of approximately 0.284 mL and a temperature of approximately 33.56 ºC. These conditions should be considered for practical applications to achieve the best corrosion protection. Based on the CCD analysis, the relationship between inhibitor concentration (Factor A), temperature (Factor B) and corrosion rate (CR) was expressed using the following regression equation derived from the ANOVA model.

The design equation derived is:

$$CR = 1.67 - 1.36A + 0.724B - 0.597AB$$

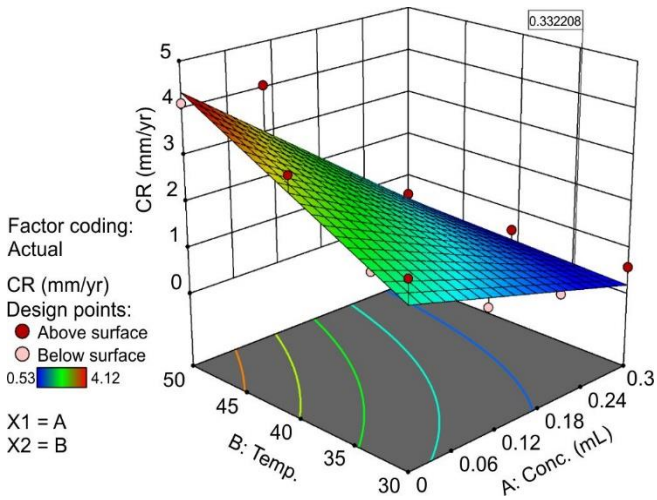

Fig. 7. Response surface of AA6063 to millet extract inhibition

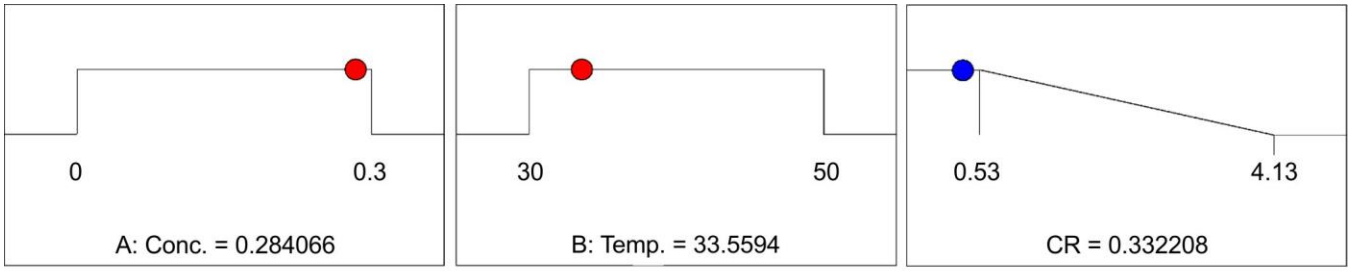

Fig. 8. Optimisation ramp plot of reduced AA6063 corrosion

This equation quantitatively describes the individual effects of concentration and temperature, as well as their interaction, on the corrosion response.

Conclusion

This study integrated electrochemical analysis with response surface methodology to evaluate and optimize the use of millet extract as a green inhibitor for AA6063 corrosion in 1 M KCl. The open circuit potential (OCP), linear sweep voltammetry (LSV) and adsorption studies confirmed the formation of a protective inhibitor film on the metal surface, while central composite design (CCD) and response surface methodology (RSM) analyses identified the optimal corrosion inhibition conditions at an inhibitor concentration of 0.284066 g and a temperature of 33.5594 ºC. Future research should explore long-term performance, synergistic combinations with other natural inhibitors and advanced surface and mechanistic characterisation using advance techniques.

ACKNOWLEDGEMENTS

The authors appreciate the support from Bells University of Technology for this research project.

CONFLICT OF INTEREST

The authors declare that there is no conflict of interests regarding the publication of this article.

DECLARATION OF AI-ASSISTED TECHNOLOGIES

During the preparation of this manuscript, the authors used an AI-assisted tool(s) to improve the language. The authors reviewed and edited the content and take full responsibility for the published work.

REFERENCES

1. E.S.M. Sherif, I.A. Alnaser and A.T. Abbas, *Sci. Eng. Compos. Mater.*, **31**, 20240031 (2024); https://doi.org/10.1515/secm-2024-0031
2. A. Dashti, M.H. Shaeri, R. Taghiabadi, F. Djavanroodi, F.V. Ghazvini and H. Javadi, *Materials*, **11**, 2419 (2018); https://doi.org/10.3390/ma11122419
3. D. Prabhu and P. Rao, *Int. J. Corros.*, **2013**, 945143 (2013); https://doi.org/10.1155/2013/945143
4. P. Kwolek, K. Dychtoń, B. Kościelniak, A. Obłój, A. Podborska and M. Wojnicki, *Metals*, **12**, 250 (2022); https://doi.org/10.3390/met12020250
5. A. Rotibi, K. Adesina and S. Abegunde, *World J. Adv. Eng. Technol. Sci.*, **6**, 40 (2022); https://doi.org/10.30574/wjaets.2022.6.1.0063
6. N. Raghavendra and J.I. Bhat, *Period. Polytech. Chem. Eng.*, **62**, 351 (2018); https://doi.org/10.3311/PPch.10686
7. A. Kumar and A. Thakur, Overview of the Properties, Applicability, and Recent Advancements of Some Natural Products used as Potential Inhibitors in Various Corrosive Systems. In: Handbook of Research on Corrosion Sciences and Engineering, IGI Global, pp. 275-310 (2023).
8. J. Garg, M.N. Chiu, S. Krishnan, K. Chawla, R.K. Gupta, S.K. Boda and M.C. Gupta, *Appl. Biochem. Biotechnol.*, **196**, 1008 (2024); https://doi.org/10.1007/s12010-023-04570-2
9. N. Raghavendra and J.I. Bhat, *J. Phys. Sci.*, **29**, 77 (2018); https://doi.org/10.21315/jps2018.29.1.6
10. O. Sanni, J. Ren and T C. Jen, Exploring the Potential Role of *Prunus domestica* in Corrosion Inhibition of AA6063-T5 Aluminium Alloy in Sodium Chloride Media, In: ASME International Mechanical Engineering Congress and Exposition, **86656**, p. V003T03A030 (2022).
11. S. Mustapha, R. Elabor, A.T. Amigun, A.A. Olajire, O.O. Joseph and A.A. Faremi, Phytochemicals/Plant Extracts as Corrosion Inhibitors for Zinc in Various Electrolytes. In: Phytochemistry in Corrosion Science, CRC Press, pp. 263-295 (2024).
12. E.M.S. Hassani, R. Salim, E. Ech-chihbi, H. Zarrok, M. Ebn Touhami and A. Dafali, *Sci. Rep.*, **15**, 12164 (2025); https://doi.org/10.1038/s41598-025-93419-1
13. I.A.W. Ma, S. Ammar, S.S.A. Kumar, K. Ramesh and S. Ramesh, *J. Coat. Technol. Res.*, **19**, 241 (2022); https://doi.org/10.1007/s11998-021-00547-0
14. Z. Aribou, M. Ouakki, F. El Hajri, E. Ech-chihbi, I. Saber, Z. Benzekri, S. Boukhris, M.K. Al-Sadoon, M. Galai, J. Charafeddine and M. Ebn Touhami, *Int. J. Electrochem. Sci.*, **19**, 100788 (2024); https://doi.org/10.1016/j.ijoes.2024.100788
15. L. Chahir, F. Benhiba, N. Abad, M. El Azzouzi, H. Zarrok, M. Ebn Touhami and A. Dafali, *J. Electrochem. Sci. Eng.*, **14**, 275 (2024); https://doi.org/10.5599/jese.2177
16. Y. Li, Z. Bai, L. Xing, X. Zhang, Y. Wang and J. Zhang, *Appl. Sci.*, **14**, 2350 (2024); https://doi.org/10.3390/app14062350
17. L. Guo, M. Zhu, Z. He, Y. Wang, X. Zhang and J. Li, *Langmuir*, **38**, 3984 (2022); https://doi.org/10.1021/acs.langmuir.1c03289
18. M.A. Deyab, Q. Mohsen, E. Bloise, M.R. Lazzoi and G. Mele, *Sci. Rep.*, **12**, 7579 (2022); https://doi.org/10.1038/s41598-022-11598-7
19. J. Li, Z. Xu, Y. Li, X. Wang, H. Zhang and Y. Wang, *J. Mater. Sci.*, **56**, 8689 (2021); https://doi.org/10.1007/s10853-020-05733-w
20. S. Kalam, S.A. Abu-Khamsin, M.S. Kamal and S. Patil, *ACS Omega*, **6**, 32342 (2021); https://doi.org/10.1021/acsomega.1c04661
21. M. Vigdorowitsch, A. Pchelintsev, L. Tsygankova and E. Tanygina, *Appl. Sci.*, **11**, 1 (2021); https://doi.org/10.3390/app11178078
22. A. Abin-Bazaine, A.C. Trujillo and M. Olmos-Marquez, in eds.: M. Ince and O.K. Ince, Adsorption Isotherms: Enlightenment of the Phenomenon of Adsorption, In: Wastewater Treatment, IntechOpen (2022); https://doi.org/10.5772/intechopen.104260